energy&fuels

pubs.acs.org/EF

Article

Hydroconversion for Hydrocarbon Generation of Highly Overmature Kerogens under Fischer−Tropsch Synthesis Conditions

Kang Li, Hong Lu,* Zhongfeng Zhao, Ping'an Peng, and Chang Samuel Hsu*

Cite This: *Energy Fuels* 2021, 35, 7808−7818

Read Online

ACCESS | Metrics & More | Article Recommendations

ABSTRACT: In order to explore the possibility of continuous hydrocarbon generation from highly mature organic matter, a series of simulation experiments of hydroconversion of highly over mature Yuertusi kerogen were conducted under Fischer−Tropsch synthesis conditions, that is, with native iron plus water for hydrogen supply. Under temperatures of 400−600 °C and a pressure of 50 MPa, very high yields of gaseous and liquid hydrocarbons were generated above 500 °C in the series of kerogen iron plus water, compared with three control experimental series of kerogen alone, kerogen plus water, and kerogen plus iron, in which the total hydrocarbon yields were ∼30 times higher than that of kerogen alone. The main mechanism is that large amount of hydrogen produced by the reaction of iron with water at high temperatures, which promotes the pyrolysis and depolymerization of kerogen macromolecules and CO_2 Fischer−Tropsch-type (FTT) synthesis, consequently producing liquid and gaseous hydrocarbons in high yields. The results were confirmed by performing another experiment of highly over mature kerogen with low sulfur of Permian Dalong Formation in the Sichuan Basin. The consistent results between the two kerogens indicated the feasibility of the hydroconversion on highly over mature kerogens. The hydroconversion method employed in this study is expected not only to largely increase the hydrocarbon production of kerogen, oil shale, coal, asphaltene, and other macromolecular organic matter upstream, but also has great significance to the refining and processing of heavy oils and fossil-fuel tailings downstream.

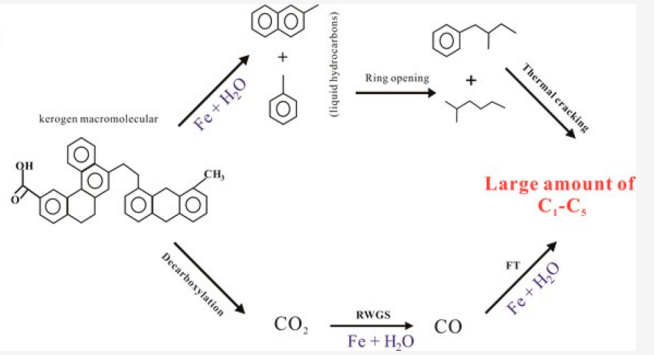

1. INTRODUCTION

Kerogen, which is an insoluble macromolecular organic matter dispersed in sedimentary rocks, is the most abundant form of organic matter on Earth. It is mainly composed of C/H/O/N/S elements and is considered to be the main source of petroleum and natural gas.[1] The evolution of kerogen can be divided into three stages during the burial of organic sediments: the immature stage (diagenesis, R_o < 0.5%), which involves the conversion of biopolymers of deposited organic matter in the presence of water and minerals into geopolymers under thermal stress compacted into sedimentary rock; the mature stage (catagenesis, 0.5% < R_o < 2.0%), which involves the thermal breakdown of geopolymers (kerogen) into petroleum oil and wet gas, which is the main stage of hydrocarbon generation; and the highly overmature stage (2.0% < R_o < 4.0%), which involves the alteration of residual kerogen after hydrocarbon release. If the kerogen exposed to extreme heat, such as proximity of magma, it would go through a metamorphic path called metagenesis to form carbon residue (pyrobitumen), along with methane generation.[2−4] Although the potential of hydrocarbon generation of kerogen in the highly overmature stage is low, there are still significant amounts of residual organic carbons left after the last stage of hydrocarbon generation. Therefore, if the highly overmature kerogen can continuously generate hydrocarbons by some effective hydroconversion or thermal conversion means, it would be of great significance for the secondary utilization of fossil fuel residues, such as oil shales upstream and crude oil distillation bottoms downstream.

Water can serve as an effective solvent for organic matter and can be used as a good reaction medium to realize the conversion of fossil fuel resources to small hydrocarbon molecules.[5,6] The conversion of kerogen, oil shale, bitumen and coal tar under high temperature (or supercritical) water or steam conditions has been studied extensively. In these studies, higher yields of hydrocarbons were obtained compared to the conditions in the absence of water.[7−10] However, the degree of conversion is dependent on the H/C atomic ratio of the initial reactant: the lower the H/C atomic ratio, the more difficult is the reaction to

Received: January 25, 2021
Revised: April 5, 2021
Published: April 26, 2021

Table 1. Geochemical Parameters of the Yuertusi and Dalong Kerogens

sample	TOC (%)	S_1 (mg/g kerogen)	S_2 (mg/g kerogen)	S_3 (mg/g kerogen)	T_{max} (°C)	HI (mg/g TOC)	OI (mg/g TOC)
Yuertusi	57	1.42	11.0	16.04	579	18	28
Dalong	76	0.74	4.05	15.47	606	5	20

proceed. Moreover, the hydroconversion of reactant is negligible, because of the chemical involvement of water molecules.[9,10] Therefore, in order to increase the hydrocarbon production, additional hydroconversion is required.

The hydroconversion refers to the molecules in fossil fuels that are split and/or saturated with hydrogen gas to generate valuable hydrocarbons, including hydrocracking, hydropyrolysis, hydrogenation, hydrogenolysis, hydroisomerization, etc.[11,12] Hence, hydrogen is important for the conversion of reactants into valuable hydrocarbons. At present, there are several approaches to realize the deep hydroconversion of fossil fuels with water as a reaction medium. At first, hydrogen is produced from steam-methane reforming (SMR), which is the most popular method in petroleum refining. Instead of using methane as the feed, naphtha or natural gas can also be used as the feed. In the second approach, CO or H_2/CO mixed gas is added with H_2O, and the hydrogenation of reactants occurs by water−gas shift (WGS) reaction.[13,14] However, in the upstream applications, a large supply of gas would be required, in quantities ∼15−20 times greater than the molar mass of organic matter. Thus, the first two approaches cannot be handled in large scale, because of the high price and strict storage conditions of H_2 and CO. Another approach is the hydroconversion of fossil materials such as kerogen, bitumen, and coal tar by redox reaction between active metals and water.[15−18] For example, Fedyaeva and Vostrikov[16] explored the catalysis effect of adding metal zinc and aluminum on the conversion of bitumen under supercritical water conditions. Good results were obtained with improved yields of liquid hydrocarbons and volatile products, which was mechanistically attributed to hydrogen generated by the reaction of active metals and H_2O. This method is easy to operate, safe and convenient, and can effectively perform the hydroconversion of fossil fuels.

Compared with zinc, aluminum, and other active metals, iron is more abundant in the crust, less expensive, more stable, and environmentally friendly. A large amount of hydrogen produced by iron and water at high temperatures can provide sufficient hydrogen supply for hydroconversion.[19−21] A series of hydroconversion experiments for biomass macromolecules, unsaturated hydrocarbons, and the synthesis of hydrocarbons from inorganic carbon sources such as CO_2 and CO were performed using iron plus water; the results showed that this approach is an effective hydroconversion method for hydrocarbon generation.[20,22−24] The coordination of iron and H_2O can greatly improve the yield of biomass crude oil (bio-oil), indicating that the addition of iron under hydrothermal conditions is feasible to promote the hydroconversion of macromolecular organic matter.[24] However, only few detailed studies have been done to explore the hydroconversion of fossil fuel resources for hydrocarbon generation by the coordination of iron and water.

Kerogen is the main source of crude oil and natural gas. However, for the highly mature kerogen, although with a large amount of residual organic carbon, the hydrocarbon generation ability is very poor. Based on the above considerations, we investigated the influence of iron plus water on the hydrocarbon generation of highly overmature Yuertusi/Dalong kerogens and the hydrocarbon generation mechanism in the temperature range of 400−600 °C, under a fixed pressure of 50 MPa. In order to compare the effect of hydroconversion on the two kerogens with iron plus water, three additional experiments of kerogen only, kerogen+H_2O, and kerogen+Fe were performed as controls for comparison.

2. SAMPLES AND EXPERIMENTS

2.1. Samples. The source rocks of Yuertusi and Dalong were collected from the Yuertusi Formation in Dongergou section of Tarim Basin and Dalong Formation in Wangcang section of Sichuan Basin, both in China. They were first cleaned and crushed to 200 mesh, and then Soxhlet-extracted with a solvent mixture of dichloromethane/methanol (9:1) for 72 h to remove soluble bitumen. After extraction, the samples were treated with hydrochloric acid to remove the carbonate minerals at 80 °C for 8 h and then washed with deionized water to pH values close to 7 after removing the HCl solution, followed by further treatment with HF/HCl (1:1) to remove silicate minerals at 80 °C for 8 h. After removing HF/HCl, the sample was treated again with HCl to remove the remaining inorganic materials, then the HCl was removed and cleaned again. The above procedure was repeated, then Soxhlet extraction was performed for 72 h to obtain the kerogen.[8]

The basic geochemical data of Cambrian Yuertusi and Permian Dalong kerogens (Table 1) showed that a high abundance of residual organic carbon (TOC = 57% and 76%) can be served as the material basis of our catalytic hydroconverion experiments. However, very low hydrogen index (HI = 18 and 5 mg/g TOC) and S_2 (11and 4 mg/g kerogen) values indicated that they have almost no ability to regenerate hydrocarbons. The values of commonly used maturity indicator R_o are 2.2% and 2.4%, indicating that they are highly mature or overmature.[25,26] The nuclear magnetic resonance spectroscopy (^{13}C NMR, Figure 1) showed that they were mainly composed

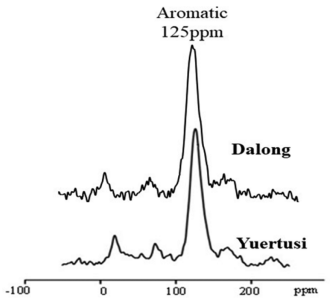

Figure 1. Solid ^{13}C NMR spectrum of Yuertusi and Dalong kerogens.

of aromatic carbons (92−150 ppm), and the proportion of aliphatic carbons was very small (0−62 ppm), consistent with the structure of highly mature kerogens.[27]

The iron powder used in this study was purchased from Alfa Company, with a purity of >99%; pure deionized water was used in the experiments.

2.2. Gold Capsules Reactor. All pyrolysis experiments were conducted in a set of gold capsules (6 mm outer diameter, 0.25 mm wall thickness, and 60 mm length). The empty capsules

https://doi.org/10.1021/acs.energyfuels.1c00284
Energy Fuels 2021, 35, 7808−7818

Table 2. Yields of Gaseous, Light-Liquid Hydrocarbons (C_6−C_{14}) and Heavy-Liquid Hydrocarbons (C_{14+}), and Inorganic Gases from Pyrolysis Experiment of Yuertusi Kerogen

	Yield (mg/g TOC)											
series[a]	CH_4	C_2H_6	C_3H_8	C_4H_{10}	C_5H_{12}	C_1−C_5	C_6−C_{14}	C_{14+}	total HC[b]	CO_2	CO	H_2
K-400	0.36	0.12	0.03	0.00	0.00	0.51	0.00	0.00	0.51	184.20	0.00	0.02
K-430	0.93	0.22	0.03	0.00	0.00	1.18	0.00	0.00	1.18	178.69	0.00	0.01
K-450	1.46	0.29	0.04	0.00	0.00	1.79	0.03	0.00	1.82	189.54	0.00	0.02
K-500	19.20	0.49	0.00	0.00	0.00	19.69	0.00	0.00	19.69	212.59	0.00	0.02
K-530	28.34	0.72	0.00	0.00	0.00	29.06	0.05	0.00	29.11	215.16	0.00	0.18
K-550	34.28	0.61	0.00	0.00	0.00	34.89	0.1	0.00	34.90	271.47	0.00	0.04
K-600	51.99	1.42	0.21	0.05	0.00	53.67	0.16	0.00	53.83	238.06	0.00	0.41
K+H_2O-400	0.37	0.14	0.04	0.01	0.00	0.56	0.00	0.00	0.56	184.12	0.00	0.13
K+H_2O-430	0.72	0.26	0.08	0.01	0.01	1.08	0.00	0.00	1.08	207.75	0.00	0.10
K+H_2O-450	1.09	0.33	0.07	0.01	0.01	1.52	0.05	0.00	1.57	207.16	0.00	0.12
K+H_2O-500	18.13	1.70	0.07	0.00	0.00	19.90	0.08	0.00	19.98	257.44	0.00	0.50
K+H_2O-530	23.51	1.84	0.06	0.00	0.00	25.41	0.00	0.00	25.41	265.54	0.00	0.84
K+H_2O-550	33.58	1.96	0.04	0.00	0.00	35.59	0.22	0.00	35.81	305.25	0.00	1.25
K+H_2O-600	49.27	1.75	0.00	0.00	0.00	51.02	0.00	0.00	51.02	340.70	0.00	2.43
K+Fe-400	1.75	0.81	0.12	0.03	0.00	2.71	0.1	0.00	2.72	0.74	4.46	2.82
K+Fe-430	3.91	1.95	0.59	0.13	0.13	6.71	0.26	0.00	6.97	38.96	7.10	2.45
K+Fe-450	6.51	3.13	1.26	0.53	0.15	11.58	0.30	0.00	11.88	71.40	6.52	1.62
K+Fe-500	51.54	25.37	8.06	4.38	0.92	90.27	0.26	0.00	90.53	33.61	0.00	0.19
K+Fe-530	61.17	17.73	6.96	2.66	0.49	89.00	0.6	0.00	89.06	17.28	0.00	0.27
K+Fe-550	79.35	15.59	3.72	1.08	0.23	99.99	0.00	0.00	99.99	5.49	0.00	0.33
K+Fe-600	93.73	3.08	0.04	0.04	0.00	96.89	0.2	0.00	97.09	0.76	0.00	0.63
K+Fe+H_2O-400	4.89	3.20	1.76	0.73	0.21	10.79	4.96	0.00	15.75	0.00	5.80	31.85
K+Fe+H_2O-430	12.82	7.64	6.17	4.72	2.00	33.36	1.76	9.08	44.2	0.00	6.20	30.42
K+Fe+H_2O-450	21.51	12.68	11.51	9.85	4.04	59.59	2.51	48.88	110.98	0.52	6.72	31.36
K+Fe+H_2O-500	151.95	132.61	182.37	89.07	20.66	576.66	196.19	226.73	999.58	0.16	12.30	34.03
K+Fe+H_2O-530	178.20	179.89	229.21	96.57	14.04	697.91	207.66	140.36	1045.93	0.00	11.50	29.90
K+Fe+H_2O-550	197.03	213.70	238.68	66.14	7.15	722.70	161.16	58.70	942.56	0.28	7.20	34.97
K+Fe+H_2O-600	428.49	473.92	63.56	5.01	0.35	971.32	119.76	25.61	1116.08	0.29	2.60	30.13

[a]Legend: K, kerogen; K+H_2O, kerogen plus water; K+Fe, kerogen plus iron; K+Fe+H_2O, kerogen plus iron and water. The numbers denote heating temperature (in °C). [b]Total HC = the total amount of gas hydrocarbons, and light- and heavy-liquid hydrocarbons.

were welded at one end before loading the sample; Then kerogen and equal amounts of deionized water and iron powder with a total mass of ∼200 mg were loaded. After the reactants were all loaded, the open end of each capsule was purged with argon for 15 min to remove the air in the capsule before being squeezed with pliers to form an initial seal, which was subsequently welded in the presence of argon. During welding, two-thirds of the gold tube was immersed in water to prevent the sample from heating. The sealed capsule was put in hot water for leak testing. The capsule was well-sealed if no bubbles appeared.

In order to analyze the gas and liquid products separately, another set of capsules with the same sample loading were prepared for parallel experiments under the identical conditions.

2.3. Heating of Capsules in Autoclaves. The samples in the sealed capsules were heated in a furnace with 15 independent autoclaves, maintained at a constant pressure of 50 MPa to keep the internal and external pressure balance of the capsules. The detailed procedures were described in other literatures.[28] The heating process was from ambient temperature to 600 °C at 20 °C/h, the autoclaves were taken at 400, 430, 450, 500, 530, 550, and 600 °C, respectively. After each autoclave was taken out of the heating furnace, it was quenched in a cold water bath. After cooling to room temperature, the capsule was checked for leakage before being weighed.

2.4. Gas Analyses. The gold capsule was placed in the vacuum glass system of a fixed volume. Under the closed condition, the sealed gas was completely released by a needle piercing and then introduced into GC for quantitative analysis.[8] The GC is equipped with seven valves, eight columns, and three detectors, in which the FID detector analyzed gaseous hydrocarbons (C_1−C_5) using helium as a carrier gas, the TCD detector analyzed H_2 using nitrogen as a carrier gas, and another TCD detector analyzed other inorganic gases (CO, CO_2 and H_2S) using helium as a carrier gas.[29] The GC oven temperature was initially held at 60 °C for 5 min, ramped to 130 °C at 15 °C/min, then to 180 °C at 25 °C/min, and held at the final temperature for 4 min. The amounts of the gas components in capsules were determined from the FID and TCD responses calibrated with gas standards.

2.5. Analysis of Light Liquid Hydrocarbons (C_6−C_{14}). In order to better understand the process of kerogen pyrolysis, the light liquid hydrocarbon (C_6−C_{14}) compounds in the gold tubes from another set were quantitatively analyzed after releasing gaseous components. The detailed procedures are as follows. First, an internal standard solution (1.83 mg deuterated *n*-C_{24} dissolved in 4 mL of frozen *n*-pentane) was prepared, then 50 μL of internal standard solution and 2 mL of frozen *n*-pentane were added into each 8 mL vial. The gold tube was pierced below the level of *n*-pentane with a steel needle, and the vial was sealed immediately after releasing gases and to avoid volatility loss of C_5+ components and left for 12 h. Then ultrasonic treatment was performed three times for 10 min each time, the 8 mL vials were allowed to settle for 12 h until the solution became clear.[30] The *n*-pentane extract was transferred to a 2 mL vial and

https://doi.org/10.1021/acs.energyfuels.1c00284
Energy Fuels 2021, 35, 7808−7818

analyzed using an Agilent Model 6890 system fitted with a CP-Si5CB column (50 m × 0.32 mm × 0.4 um) under nitrogen as a carrier gas. The oven temperature was programmed from 40 °C (held for 5 min) to 290 °C (held for 30 min) at a heating rate of 4 °C/min.

In view of the uncommon distribution patterns of light liquid hydrocarbons from GC, the obtained extracts were further qualitatively analyzed by gas chromatography−mass spectrometry (GC-MS) to identify the compounds generated during pyrolysis. The GC-MS analyses were conducted using a DSQ-II mass spectrometry interfaced to a Hewlett Packard Model HP5890 GC gas chromatograph system, using helium as a carrier gas. The GC oven temperature was initially at 40 °C for 5 min, raised from 40 °C to 290 °C at 4 °C/min, and held at 290 °C for 30 min.

2.6. Analysis of Heavy Liquid Hydrocarbons (C_{14+}). After the GC analyses for gases and light liquid hydrocarbons, the solid residue in the gold capsule was extracted with dichloromethane to separate the soluble organic matter from the residual solid, and the soluble organic matter was weighed as the yield of the heavy liquid hydrocarbons (C_{14+}). The C_{14+} components were also qualitatively analyzed by GC-MS using *n*-hexane as the solvent. The GC oven temperature was initially at 80 °C for 2 min, then increased to 300 °C at 3 °C/min held at 300 °C for 20 min.

2.7. X-ray Diffraction Analysis of Solid Residue. The composition of solid residues in four groups was analyzed by X-ray diffraction (XRD), equipped with a Ni filter and Cu Kα radiation (40 kV and 40 mA). The diffraction patterns were collected from 2° to 55° 2θ at a scanning rate of 3° 2θ min^{-1}.

3. RESULTS

According to the above experimental procedures, the yields of gaseous hydrocarbons, light (C_6−C_{14}) and heavy liquid hydrocarbons (C_{14+}), and inorganic gas generated from the pyrolysis of Yuertusi kerogen in four series of experiments, are summarized in Table 2.

3.1. Yield and Composition of Gas Products. *3.1.1. Inorganic Gases.* The inorganic gases from the pyrolysis of Yuertusi kerogen were mainly CO_2 and increased from 184.2 mg/g TOC to 271.5 mg/g TOC from 400 to 600 °C, indicating that CO_2 retained in the kerogen matrix was expelled at high temperatures.[31] The yields of H_2 (0.01−0.41 mg/g TOC) were very low over the entire temperature range. The compositions and yields of inorganic gas in the kerogen+H_2O series were similar to that of the kerogen series, but slightly higher CO_2 yields from 184 mg/g TOC to 340 mg/g TOC were obtained with the temperatures increasing from 400 °C to 600 °C, reflecting additional CO_2 being pushed off the kerogen matrix by added water.[32] The yields of H_2 (0.12−2.43 mg/g TOC) was slight higher, compared with kerogen alone, probably because water was decomposed at high temperature to generate hydrogen.[30]

The yields of CO_2 (0.7−71.4 mg/g TOC) decreased significantly in the kerogen+Fe series, along with the formation of gaseous hydrocarbons at higher temperatures. Higher amount of H_2 (1.62−2.82 mg/g TOC) appeared at temperatures below 500 °C and decreased significantly when temperatures were >500 °C, accompanied by increases in gaseous hydrocarbons.

The yields of CO_2 decreased to almost zero over the entire temperature range in the kerogen+Fe+H_2O series. Significant amounts of H_2 (29.9−34.97 mg/g TOC) were detected due to iron reacting with water. It was found that iron reacted with water at high temperature to form magnetite (Fe_3O_4), detected by the XRD analysis of the solid residue, and released H_2 (see Figure 2). Some amounts of CO were also found in this experimental series (2.6−12.3 mg/g TOC).

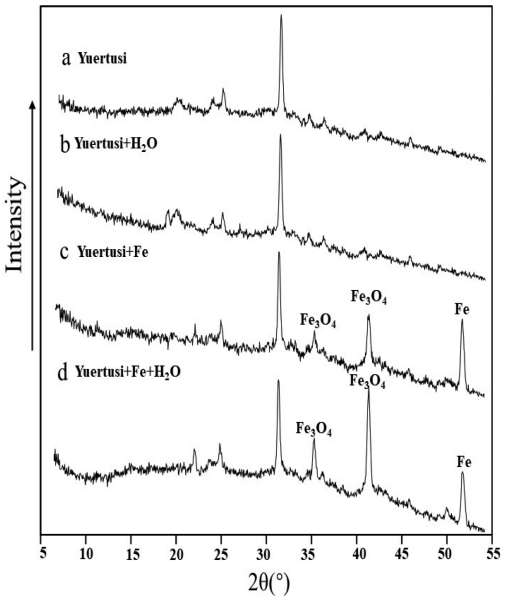

Figure 2. XRD analysis of solid residues of Yuertusi kerogen in four series (the peak at 31° corresponds to quartz after the removal of carbonates and silicates).

3.1.2. Gaseous Hydrocarbons (C_1−C_5). Only small amounts of gaseous hydrocarbons were generated from the pyrolysis of the kerogen and kerogen+H_2O series, with $\sum C_{1-5}$ = 0.51−53.67 mg/g TOC and $\sum C_{1-5}$ = 0.56−51.02 mg/g TOC (Table 2, Figure 3), respectively, over the entire temperature range of 400−600 °C, dominated by methane, and its yields increased

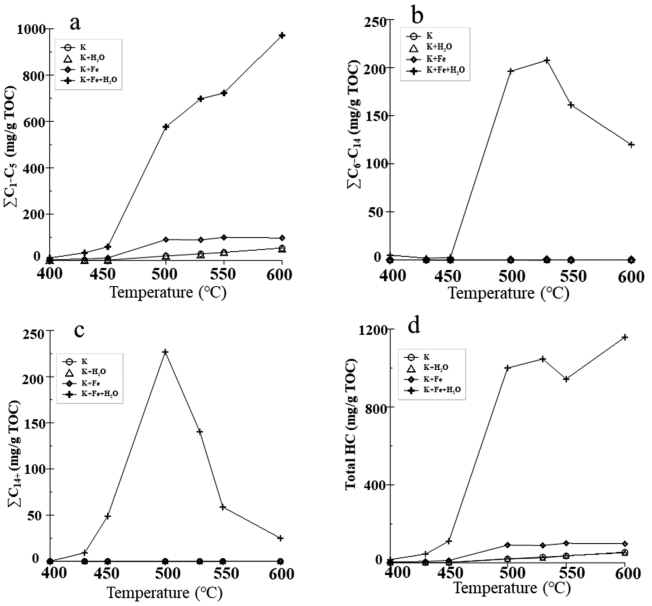

Figure 3. Quantities of (mg/g TOC) of hydrocarbons during pyrolysis of Yuertusi kerogen: (a) gaseous hydrocarbons ($\sum C_1$−C_5); (b) light-liquid hydrocarbons (C_6−C_{14}); (c) heavy-liquid hydrocarbons (C_{14+}); and (d) total amount of hydrocarbons ($\sum C_1$−C_5 + C_6−C_{14} + C_{14+}).

https://doi.org/10.1021/acs.energyfuels.1c00284
Energy Fuels 2021, 35, 7808−7818

with increasing temperature. The total gaseous hydrocarbons of the kerogen+Fe series, $\sum C_{1-5}$ = 2.71−99.99 mg/g TOC, were at least 2 times of the kerogen series at corresponding temperatures. In this series, not only methane (1.75−93.73 mg/g TOC) increased, compared to the kerogen series, but also ethane (0.81−25.37 mg/g TOC), propane (0.12−8.06 mg/g TOC), butane (0.03−4.38 mg/g TOC), and pentane (0−0.92 mg/g TOC) were present in fairly higher amounts.

The yields of total gaseous hydrocarbons in the kerogen+Fe +H_2O series, $\sum C_{1-5}$ = 10.79−971.32 mg/g TOC, increased 18−33 times, compared with the kerogen series at corresponding temperatures (Table 2, Figure 3). Methane (4.89−428.49 mg/g TOC) and ethane (3.20−473.92 mg/g TOC) increased consistently with increasing temperatures, but the yields of propane (1.76−238.68 mg/g TOC), butane (0.73−96.57 mg/g TOC), and pentane (0.21−20.66 mg/g TOC) increased initially with temperature then decreased after peaks at 550, 530, and 500 °C, respectively. The high carbon number hydrocarbons decrease more pronounced above the peak temperature. Besides, the total amounts of gaseous hydrocarbons ($\sum C_{1-5}$) increased slowly below 450 °C (10.79−59.59 mg/g TOC), but increased rapidly above 500 °C (576.66−971.32 mg/g TOC).

3.2. Yields and Compositions of Liquid Hydrocarbons. Because of the high maturity of the Yuertusi kerogen, no or minor liquid products were obtained in the three-control-experiment series of kerogen, kerogen+H_2O, and kerogen+Fe, but significant amounts of liquid products were obtained in the series of kerogen+Fe+H_2O, especially above 500 °C (see Table 2, as well as Figure 3). The liquid hydrocarbon yields first increased to the maximum values then decreased significantly as the temperature increased. Specifically, high yields of light hydrocarbons C_{6-14} were obtained at 500 °C (196.19 mg/g TOC), 530 °C (207.66 mg/g TOC), 550 °C (161.16 mg/g TOC), and 600 °C (119.76 mg/g TOC), while high yields of C_{14+} were obtained at 500 °C (226.73 mg/g TOC), 530 °C (140.36 mg/g TOC), and 550 °C (58.70 mg/g TOC), although C_{6-14} (1.76−4.96 mg/g TOC) and C_{14+} (0−48.88 mg/g TOC) have relatively smaller yields below 450 °C. This indicated the liquid hydrocarbon generation threshold near 500 °C.

In the GC quantitative analysis of light liquid hydrocarbons (C_6-_{14}), we noticed that the chromatographic distribution pattern of C_{6-14} was obviously different than that of conventional low-maturity kerogen. Therefore, in order to identify the components, the liquid products of light (C_6-C_{14}) and heavy (C_{14}+) hydrocarbons were qualitatively analyzed by GC-MS. The results showed that light hydrocarbons (C_6-_{14}) and heavy hydrocarbons (C_{14}+) are mainly composed of polycyclic aromatic hydrocarbons compounds. Specifically, light hydrocarbons (C_6-_{14}) are mainly composed of ethyl-benzene, xylene, methyl-indan, and other alkyl one-ring aromatic hydrocarbons; naphthalene, methyl-naphthalene, biphenyl, methyl-biphenyl, and other alkyl two-ring aromatic hydrocarbons; and phenanthrene (Figure 4). The heavy liquid hydrocarbons of C_{14+} are mainly composed of 2H-pyrene, pyrene, ethyl-pyrene, ethyl-benzanthracene of four-ring aromatic hydrocarbons and dibenzophenylene (five-ring) (Figure 5).

3.3. Applicability of Iron Plus Water for Hydroconversion. In order to verify the validity and feasibility of our hydroconversion method for highly overmature kerogens, another kerogen of Permian Dalong Formation ($R_o \approx 2.4\%$) in the Sichuan Basin[26] was used as the reactant to perform the simulation experiments under the same experimental conditions. The results are listed in Table 3 and Figure 6, which are similar to that of Yuertusi kerogen.

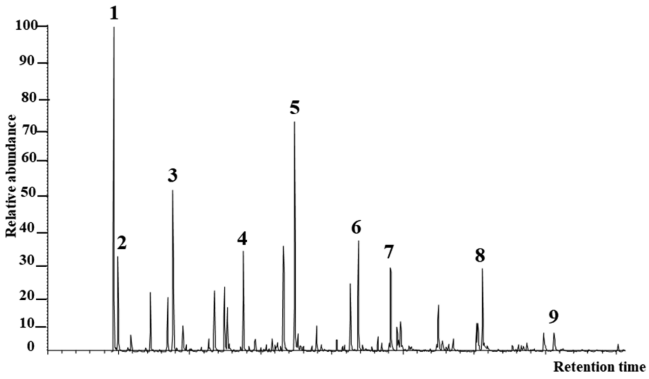

Figure 4. Gas chromatograms of various types of aromatic hydrocarbon compounds in light hydrocarbons (C_{6-14}) produced at 530 °C in the kerogen plus Fe and H_2O series. Legend: **1** = ethyl-benzene (C_8H_{10}); **2** = *o*-xylene (C_8H_{10}); **3** = 1-ethyl-3-methyl -benzene (C_9H_{12}); **4** = methyl-indan ($C_{10}H_{12}$); **5** = naphthalene ($C_{10}H_8$); **6** = 2-methyl-naphthalene ($C_{11}H_{10}$); **7** = biphenyl ($C_{12}H_{10}$); **8** = l,2-methyl-bipheny ($C_{13}H_{12}$); and **9** = phenanthrene ($C_{14}H_{10}$).

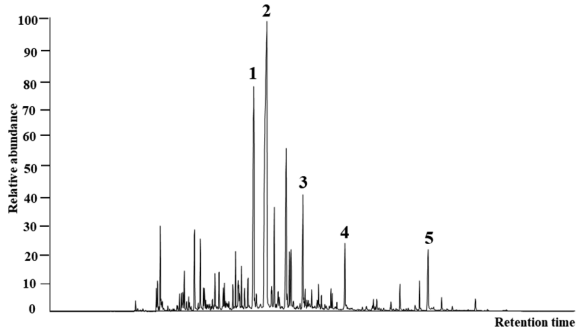

Figure 5. Gas chromatograms of various types of polycyclic aromatic hydrocarbon compounds in heavy hydrocarbons (C_{14+}) produced at 530 °C in the kerogen plus Fe and H_2O series. **1** = 2H-[pyrene] ($C_{16}H_{12}$); **2** = pyrene ($C_{16}H_{10}$); **3** = ethyl pyrene ($C_{17}H_{12}$); **4** = ethyl benzanthracene ($C_{20}H_{22}$); **5** = dibenzophenylene ($C_{22}H_{14}$).

Briefly, small amounts of gaseous hydrocarbons were obtained in the Dalong kerogen and the Dalong kerogen +H_2O series at 0.34−21.98 mg/g TOC and 0.28−21.95 mg/g TOC, respectively. In the kerogen+Fe series, the yields of gaseous hydrocarbons were 2.34−44.01 mg/g TOC, two times or higher than that of the kerogen series. However, in the kerogen+Fe+H_2O series, the yields of total gaseous hydrocarbons increased significantly, ranging from 9.44 mg/g TOC to 910.26 mg/g TOC, very significantly higher than that of the kerogen series. Besides, high yields of liquid hydrocarbons were also generated in the kerogen+Fe+H_2O series.

Based on the results described above, in the presence of iron and water, both Yuertusi kerogen and Dalong kerogen produced high yields of gaseous and liquid hydrocarbons, with the total yields were close to even over 1000 mg/g TOC at high temperatures above 500 °C, indicating the validity and feasibility of hydrocarbon generation by hydroconversion of iron plus water on highly mature kerogens.

4. DISCUSSIONS

4.1. Carbon Dioxide Fischer−Tropsch Synthesis for Hydrocarbon Generation. The presence of carbon dioxide in the Yuertusi/Dalong kerogen pyrolysis products indicated the

https://doi.org/10.1021/acs.energyfuels.1c00284
Energy Fuels 2021, 35, 7808−7818

Table 3. Yields (mg/g TOC) of Gaseous, Light-Liquid Hydrocarbons (C_6–C_{14}), and Heavy Liquid Hydrocarbons (C_{14+}) and Inorganic Gases from Pyrolysis Experiments of Dalong Kerogen

	Yield (mg/g TOC)											
series	CH_4	C_2H_6	C_3H_8	C_4H_{10}	C_5H_{12}	C_1–C_5	C_6–C_{14}	C_{14+}	total HC	CO_2	CO	H_2
DL-400	0.26	0.02	0.03	0.02	0.01	0.34	0.00	0.00	0.34	102.60	0.00	0.00
DL-430	0.28	0.04	0.02	0.02	0.01	0.37	0.00	0.00	0.37	110.87	0.00	0.00
DL-450	0.32	0.02	0.01	0.01	0.01	0.37	0.00	0.00	0.37	115.35	0.00	0.00
DL-500	2.98	0.07	0.00	0.00	0.00	3.05	0.00	0.00	3.05	151.54	0.00	0.00
DL-530	4.75	0.10	0.00	0.00	0.00	4.85	0.00	0.00	4.85	134.97	0.00	0.00
DL-550	7.65	0.08	0.00	0.00	0.00	7.73	0.00	0.00	7.73	157.61	0.00	0.00
DL-600	21.78	0.19	0.00	0.00	0.00	21.98	0.00	0.00	21.98	195.30	0.00	0.00
DL+H_2O-400	0.26	0.01	0.00	0.00	0.00	0.28	0.00	0.00	0.28	104.91	0.00	0.00
DL+H_2O-430	0.30	0.02	0.00	0.00	0.00	0.32	0.00	0.00	0.32	111.39	0.00	0.00
DL+H_2O-450	0.36	0.02	0.00	0.00	0.00	0.38	0.00	0.00	0.38	118.74	0.00	0.00
DL+H_2O-500	3.07	0.16	0.07	0.10	0.10	3.50	0.00	0.00	3.5	161.10	0.00	0.24
DL+H_2O-530	5.02	0.22	0.02	0.04	0.04	5.34	0.00	0.00	5.34	171.78	0.00	0.43
DL+H_2O-550	7.32	0.31	0.00	0.01	0.01	7.65	0.00	0.00	7.65	166.99	0.00	0.63
DL+H_2O-600	21.21	0.73	0.01	0.00	0.00	21.95	0.00	0.00	21.95	207.93	0.00	1.48
DL+Fe-400	2.08	0.23	0.01	0.00	0.00	2.34	0.00	0.00	2.34	21.30	3.89	2.75
DL+Fe-430	4.09	0.66	0.04	0.00	0.00	4.79	0.00	0.00	4.79	21.17	5.79	2.10
DL+Fe-450	6.52	1.28	0.09	0.01	0.01	7.90	0.00	0.00	7.9	28.54	7.09	1.36
DL+Fe-500	21.13	4.24	0.85	0.11	0.11	26.43	0.00	0.00	26.43	0.00	0.00	0.00
DL+Fe-530	26.05	4.82	0.78	0.06	0.06	31.77	0.00	0.00	31.77	0.00	0.00	0.12
DL+Fe-550	36.31	2.42	0.08	0.00	0.00	38.80	0.00	0.00	38.8	0.00	0.00	0.12
DL+Fe-600	43.58	0.43	0.00	0.00	0.00	44.01	0.00	0.00	44.01	0.00	0.00	0.17
DL+Fe+H_2O-400	6.74	1.92	0.56	0.22	0.00	9.44	4.71	52.16	66.31	0.10	3.84	41.65
DL+Fe+H_2O-430	17.73	6.57	3.42	2.25	0.57	30.54	6.64	32.34	69.52	3.00	3.94	46.48
DL+Fe+H_2O-450	25.05	9.84	6.99	6.99	1.98	50.85	5.82	25.91	82.58	0.25	4.77	47.84
DL+Fe+H_2O-500	143.39	132.89	173.37	103.65	18.11	571.40	147.38	202.16	920.94	0.00	9.02	35.07
DL+Fe+H_2O-530	176.33	189.27	226.62	105.32	12.03	709.56	172.72	127.77	1010.05	0.00	8.58	27.50
DL+Fe+H_2O-550	202.57	230.83	236.86	50.95	2.09	723.30	42.92	71.05	837.27	0.00	6.48	22.59
DL+Fe+H_2O-600	376.09	469.48	62.63	1.94	0.12	910.26	31.26	40.35	981.87	1.08	2.25	20.15

[a]Legend: DL, kerogen; DL+H_2O, kerogen plus water; DL+iron, kerogen plus iron; DL+Fe+H_2O, kerogen plus iron and water. The numbers denote heating temperatures in °C. [b]Total HC = the total amount of gas hydrocarbons, light and heavy liquid hydrocarbons.

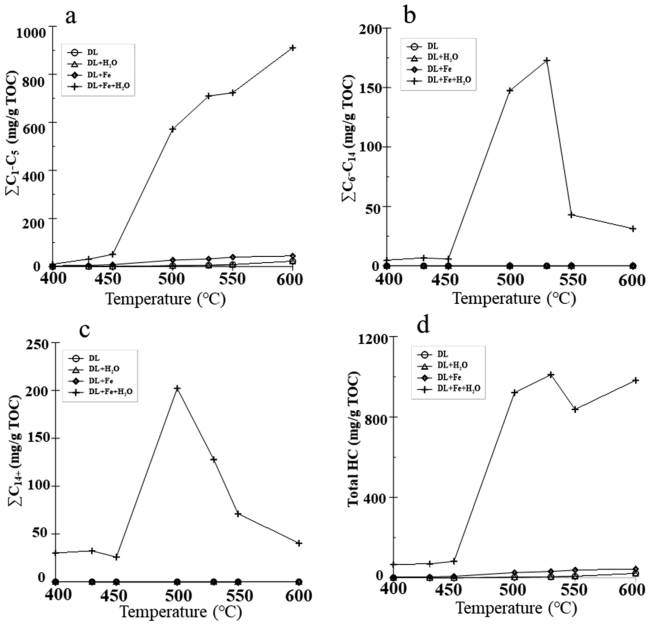

Figure 6. Quantities of (mg/g TOC) of hydrocarbons during pyrolysis of Dalong kerogen: (a) gaseous hydrocarbons ($\sum C_1$–C_5); (b) light-liquid hydrocarbons (C_6–C_{14}); (c) heavy-liquid hydrocarbons (C_{14+}); and (d) total amount of hydrocarbons ($\sum C_1$–C_5 + C_6–C_{14} + C_{14+}).

expulsion of retained carbon dioxide in the kerogen matrix.[31−34] The addition of water in the Yuertusi/Dalong kerogen+H_2O series pushed off more desorbed carbon dioxide because water occupied the adsorption sites and reduce the adsorption ability of CO_2.[32,35] However, the yields of CO_2 were significantly reduced in the Yuertusi/Dalong kerogen+Fe series, accompanied by the formation of carbon monoxide (CO) and hydrogen (H_2). These gases diminished at the temperatures above 500 °C, with the formation of higher amounts of gaseous hydrocarbons (Tables 2 and 3). CO_2 was completely depleted in the kerogen+Fe+H_2O series, more residual carbon monoxide (CO) and hydrogen (H_2) were found and larger quantities of gaseous hydrocarbons were produced. All these results indicated the CO_2 Fischer−Tropsch-type synthesis occurring in the kerogen+Fe+H_2O and kerogen+Fe series.

CO_2 Fischer−Tropsch-type synthesis (FTT) refers to the reduction of CO_2 in the presence of H_2 and transition-metal catalyst to produce methane, C_2–C_4 alkanes/alkenes and long-chain liquid hydrocarbons via carbon monoxide.[36,37] It mainly consists of two reaction steps: the reduction of CO_2 to CO through reverse water−gas shift (RWGS) reaction (eq 2) and the hydrogenation of CO to hydrocarbons by the classical FTS reaction (eq 3). Previous studies on Fe-catalyzed CO_2 FTT showed that (1) iron catalysts can catalyze both the RWGS reaction and the hydrogenation of CO, which were expected to show good performances for CO_2 FTT;[38,39] (2) The reaction products of CO_2 FTT on iron catalysts were mainly methane

https://doi.org/10.1021/acs.energyfuels.1c00284
Energy Fuels 2021, 35, 7808−7818

and C_2-C_4 gaseous hydrocarbons (including olefins and alkanes), in terms of the selectivity and activity.[40,41] For example, Dossary et al.[41] explored the hydrogenation of CO_2 with iron oxide as a catalyst, and the results showed that the products were mainly methane and C_2-C_5 gas hydrocarbons. In our reaction system of kerogen+Fe+H_2O, a large amount of H_2 was generated by Fe+H_2O at high temperatures (eq 1), which promoted the conversion of CO_2 into CO through RWGS reaction (eq 2), evidenced by the residual CO being detected (Tables 2 and 3). Subsequently, FT reaction occurred between CO and H_2 on an Fe catalyst to generate methane and C_2-C_5 gas hydrocarbons. It is worth noting that gas alkenes were not detected in our reaction system due to the unstable alkenes readily hydrogenated into saturated hydrocarbons in the presence of hydrogen.[42]

$$3Fe + 4H_2O \rightarrow Fe_3O_4 + 4H_2 \quad (1)$$

$$CO_2 + H_2 \rightarrow CO + H_2O \quad (2)$$

$$CO + 2H_2 \rightarrow (-CH_2 -) + H_2O \quad (3)$$

In addition, the CO_2 FTT could also generate long-chain liquid hydrocarbons (>C_5).[43,44] For example, Wang et al.[43] explored that, for the hydrogenation of CO_2 with Fe catalyst, the selectivity of long-chain liquid hydrocarbon is 20% when the K^+ dopant is added but little liquid hydrocarbons were obtained in the absence of dopant. Hwang et al.[44] used mesoporous carbon as support for Fe catalyst for CO_2 hydrogenation to liquid hydrocarbons, the result showed liquid hydrocarbon selectivity of 44.5%. However, in our reaction of kerogen+Fe+H_2O, no long-chain alkanes (>C_5) were found in the GC-MS analysis of kerogen+Fe+H_2O products (Figures 4 and 5), indicating that there was no long-chain liquid hydrocarbon synthesis in our reaction system. This is probably because the selectivity of the sole iron catalyst for long-chain liquid hydrocarbons was low.[37]

The yield ranges of total gaseous hydrocarbons in the Yuertusi/Dalong kerogen+Fe series were at least two times higher than that of kerogens only (see Tables 2 and 3). We believe that CO_2 FTT also occurred in the Yuertusi/Dalong kerogen+Fe series. Some studies have shown that some water exists in the kerogen pores.[45,46] Therefore, it may be expelled from the kerogen pores at high temperatures and reacted with Fe (eq 1) to produce H_2 and Fe_3O_4, which promotes the Fischer–Tropsch type synthesis of CO_2. XRD analysis of the solid residues in the kerogen+Fe series confirmed the presence of Fe_3O_4, and higher amounts of H_2 were generated (Figure 2, Tables 2 and 3), indicating the occurrence of this reaction. However, the H_2 produced is limited, because of the low concentration of water in kerogen, which limits the CO_2 FTT and the hydroconversion of kerogen, making the hydrocarbon yield much lower than that of the kerogen+Fe+H_2O series.

4.2. Generation Mechanism of Gaseous Hydrocarbon in Highly Mature Kerogens. Only small amounts of total gaseous hydrocarbons were generated from the pyrolysis of the Yuertusi/Dalong kerogen and kerogen+H_2O series over the entire temperature range, mainly dominated by methane, which is consistent with the hydrocarbon generation characteristics of highly mature kerogens (Tables 2 and 3). In the high maturity stage, methane is mainly generated by the decomposition of short-chain alkyl aromatics in kerogen, the demethylation of branched substituents, and the automatic hydrogenation of pyrolysis residues.[47]

The total yields of gaseous hydrocarbons increased significantly in the Yuertusi/Dalong kerogen+Fe+H_2O series, compared with the kerogen series, indicating that the coordination iron plus water greatly promoted the generation of gaseous hydrocarbons (see Tables 2 and 3, as well as Figures 3 and 6).

Besides the contribution of CO_2 Fischer–Tropsch-type synthesis, the hydrocracking of kerogen macromolecules is another reason for gaseous hydrocarbon generation. The ^{13}C NMR spectra of Yuertusi/Dalong kerogens showed that they are mainly composed of aromatic carbons (Figure 1). The GC-MS results of liquid hydrocarbons generated in kerogen+Fe+H_2O were mainly composed of aromatic compounds too (Figures 4 and 5). Previous studies have demonstrated that it is feasible to produce gaseous hydrocarbons in high yields by hydrocracking of fossil fuels and model compounds which are rich in polycyclic aromatic hydrocarbons (PAHs).[48−50] For example, Sanford et al. explored the hydrocarbon yield during pyrolysis of asphalt residue under the condition of N_2 and H_2; the results showed that higher yield of gaseous hydrocarbons were generated under the condition of H_2, and it can be interpreted as the PAHs generated from the asphalt residue continued to undergo hydrocracking to produce gas hydrocarbons.[48,49] Weitkamp et al.[50] proved the feasibility of hydrocracking of PAHs to gaseous hydrocarbons by model benzene compounds, indicating that benzene has undergone a ring opening cracking reaction. In our experiment of kerogen+Fe+H_2O series, a large amount of H_2 was produced from the iron and water reactions at high temperatures, which promoted the hydrocracking of kerogen macromolecules to generate liquid hydrocarbons and gas hydrocarbons. The liquid hydrocarbons continue to undergo hydrocracking to produce gaseous hydrocarbons and the yield of light- and heavy-liquid hydrocarbons decreased as the temperature increased from 500 °C to 600 °C, also indicating that the hydrocracking of liquid hydrocarbons occurred.

Based on the discussions above (Sections 4.1 and 4.2), simplified hydrocarbon generation mechanisms of the kerogens +Fe+H_2O series were proposed according to the reaction mechanisms of bitumen residue suggested by Sanford (see Figure 7).[48,49] The structural model of high mature kerogen proposed by Huang et al.[51] was selected. It mainly includes two reaction routes:

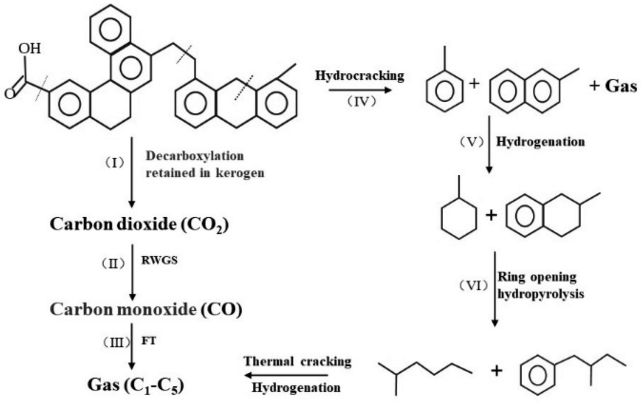

Figure 7. Simplified mechanism of hydrocarbon generation for highly mature kerogens with iron and water. (Parentheses indicate the reaction route.)

https://doi.org/10.1021/acs.energyfuels.1c00284
Energy Fuels 2021, 35, 7808−7818

Table 4. Hydrocarbon Yields Generated from Three Different Types of Carbon in Yuertusi/Dalong Kerogen at Different Temperatures under Fe + H_2O Conditions

	Yield (%)					Yield (%)			
series	total hydrocarbons	CO_2 FTS	aromatic carbon	alphatic carbon	series	total hydrocarbons	CO_2 FTS	aromatic carbon	alphatic carbon
K+Fe+H_2O-400	15.75	63.67	/[a]	0.51	DL+Fe+H_2O-400	66.31	35.11	30.86	0.34
K+Fe+H_2O-430	44.2	61.44	/[a]	1.18	DL+Fe+H_2O-430	69.52	38.06	31.09	0.37
K+Fe+H_2O-450	110.98	65.08	44.11	1.79	DL+Fe+H_2O-450	82.58	39.22	42.99	0.37
K+Fe+H_2O-500	999.58	70.28	909.61	19.69	DL+Fe+H_2O-500	920.94	49.95	867.94	3.05
K+Fe+H_2O-530	1045.93	71.67	945.20	29.06	DL+Fe+H_2O-530	1010.05	44.18	961.02	4.85
K+Fe+H_2O-550	942.56	94.60	813.07	34.89	DL+Fe+H_2O-550	837.27	53.61	775.93	7.73
K+Fe+H_2O-600	1116.08	85.08	977.33	53.67	DL+Fe+H_2O-600	981.87	69.73	890.16	21.98

[a]The slash symbol (/) denotes that the yield could not be calculated.

(1) A large amount of CO_2 retained in kerogen would be expelled (I) and can be reduced to CO through reverse water−gas shift (RWGS) reaction (II); then, the hydrogenation of CO by FT reaction occurred, generating methane and C_2−C_5 gas hydrocarbons (III);
(2) Kerogen was decomposed into some gaseous and liquid hydrocarbons through hydrocracking (IV), the liquid hydrocarbons were continuously hydrogenated to cycloalkanes (V), which would undergo ring opening (hydrogenolysis) and hydrocracking (thermal cracking under hydrogen) to generate gaseous hydrocarbons (VI).[52]

4.3. Generation Mechanism of Liquid Hydrocarbons in Highly Mature Kerogens. In our experiments, liquid hydrocarbons were only produced in the conditions of iron plus water (recall Tables 2 and 3, as well as Figures 4 and 5). Note that the liquid hydrocarbons were generated by either catalytic hydropyrolysis of kerogen or CO_2 Fischer−Tropsch type reaction. It is generally known that CO_2 Fischer−Tropsch-type reactions yield mainly aliphatic hydrocarbons, particularly gaseous, and some oxygenates. Thus, catalytic hydropyrolysis should play a greater role in the generation of liquid hydrocarbon.

High concentration of H_2 in the kerogen+Fe+H_2O series means that hydrogen is sufficient for the whole reaction, and the high pressure of 50 MPa ensures the close contact between hydrogen and kerogen. In addition, iron is likely to promote the activation of H_2 to produce active hydrogen atom and transfer to kerogen macromolecule. According to the previous studies,[48,49] we think that the mechanism of liquid hydrocarbon generated in our gold-tube closed system are as follows: C−C bond fracture occurs in the pyrolysis of kerogen at high temperatures to generate a large number of free radicals, and, in the presence of H_2, the free-radical fragments generated are stabilized, resulting in the depolymerization of kerogen macromolecules to produce liquid hydrocarbons, which are rich in aromatic compounds.

4.4. Mass Balance of Carbon Types. The total hydrocarbon yields in the Yuertusi/Dalong kerogen+Fe+H_2O series increased consistently with increasing temperature, and the yields were close to or even higher than 1000 mg/g TOC at temperatures above 500 °C, which almost realized the conversion of all the carbon in the kerogen. Hydrocarbons were generated mainly by three types of reactions: Fischer−Tropsch synthesis reaction, thermal cracking, and hydrocracking. In order to determine which type of reaction was dominant at different temperatures, it is necessary to do carbon-type equilibrium calculations.

The carbon types in the Yuertusi/Dalong kerogens can be divided into the three types according to the experimental results and the NMR spectra (see Tables 2 and 3, as well as Figure 1): CO_2; aliphatic carbons (minor amount); aromatic carbons (dominant). The hydrocarbons generated in kerogen alone or in the kerogen+H_2O series should mainly come from the thermal cracking of small amounts of aliphatic carbons. However, the hydrocarbons generated in the kerogen+Fe+H_2O series are mainly through three types of reactions: thermal cracking of aliphatic carbons, CO_2 Fischer−Tropsch-type synthesis (FTS), and the hydrocracking of aromatic carbons.

We assume that the amounts of CO_2 generated by the pyrolysis of kerogen alone are the same as that generated in the kerogen+Fe+H_2O series. Hence, the original amounts of CO_2 generated in the Yuertusi kerogen+Fe+H_2O series should also be 184.2−238.06 mg/g TOC. Under the conditions of Fe + H_2O, subtracting the amount of residual CO_2 and that converted to CO, the maximum yield range of complete conversion of CO_2 to hydrocarbons was 63.67−94.60 mg/g TOC, according to eq 4. The hydrocarbons generated from the thermal cracking of aliphatic carbons in the Yuertusi kerogen+Fe+H_2O series were 0.51−53.83 mg/g TOC, which is assumed the same as the kerogen alone. Therefore, the hydrocarbon yields generated by the hydrocracking of aromatic carbons were 44.11−977.33 mg/g TOC, which can be calculated by subtraction of the yield generated by CO_2 FTS and thermal cracking of aliphatic carbons from the total hydrocarbon yields (eq 5). Based on the same method, the contributions of three different types of carbon in Dalong kerogen to hydrocarbons under the conditions of Fe + H_2O at 400−600 °C were calculated. The maximum hydrocarbon yield generated by the CO_2 FTS would be 35.11−69.73 mg/g TOC, and the hydrocarbon yields generated by the hydrocracking of aromatic carbons were 43.36−912.14 mg/g TOC in the temperature range of 400−600 °C. The contributions of three different types of carbon-to-hydrocarbon generation at different temperatures of the two kerogens are shown in Table 4.

$$m(\mathrm{FT}) = \left(\frac{\Delta m(\mathrm{CO_2})}{44} - \frac{m(\mathrm{CO})}{28}\right) \times 16 \quad (4)$$

https://doi.org/10.1021/acs.energyfuels.1c00284
Energy Fuels 2021, 35, 7808−7818

$$m(\mathrm{HC}) = m(\mathrm{TH}) - m(\mathrm{TC}) - m(\mathrm{FT}) \quad (5)$$

where $m(\mathrm{FT})$ represents the hydrocarbon yields generated by CO_2 Fischer−Tropsch-type synthesis; $\Delta m(CO_2)$ is the difference of CO_2 yields between the kerogen alone and kerogen+Fe $+H_2O$; 44 is the molecular weight of CO_2; 28 is the molecular weight of CO; 16 is the molecular weight of CH_4; $m(\mathrm{CO})$ represents the CO yields in the kerogen+Fe+H_2O series; $m(\mathrm{HC})$ represents the hydrocarbon yields generated by the hydrocracking of aromatic carbons; $m(\mathrm{TH})$ represents the hydrocarbon yields generated by the total hydrocarbons; and $m(\mathrm{TC})$ represents the hydrocarbon yields generated by the thermal cracking of aliphatic carbons.

Table 4 shows that the calculated hydrocarbon yields generated by CO_2 FTS reaction below 450 °C are close to the measured total hydrocarbon yields, which indicates that the generation of hydrocarbons at low temperature is mainly by CO_2 FTS. Some show that the complete conversion of CO_2 is higher than the measured total hydrocarbon amount, probably due to CO_2 not being completely converted to hydrocarbons at low temperatures. As the temperature increased, the hydrocarbons generated by the hydrocracking of aromatic carbons were dominant above 500 °C.

5. CONCLUSION

In order to explore the possibility of continuous hydrocarbon generation from highly mature kerogens, two highly overmature kerogens from Yuertusi and Dalong formations were used as reactants to explore the possibilities of hydrocarbon generation through hydroconversion in the presence iron and water at the temperature range from 400 °C to 600 °C, under a fixed pressure of 50 MPa. The main conclusions are as follows:

(1) Iron plus water significantly promotes the hydroconversion of highly mature kerogen to generate liquid and gaseous hydrocarbons in high yields, realizing the conversion of most residual carbons in kerogen into hydrocarbons.
(2) Under the conditions of iron plus water, the generation of hydrocarbons was dominant by CO_2 FTS below 450 °C, but the generation of aromatic carbons was dominant by hydrocracking above 500 °C.
(3) Residual carbon monoxide found in the kerogen plus iron and water experiments provides evidence of abiogenic hydrocarbon generation from reduced CO_2 through Fischer−Tropsch-type reactions via carbon monoxide.
(4) The method of kerogen with addition of iron plus water in the sealed gold-tube system provides a feasible catalytic hydrocracking and Fischer−Tropsch-type reaction route for hydrocarbon generation from highly overmature kerogens that have a minimum potential of hydrocarbon generation. Similar approach might be applied to the iron-catalyzed Fischer−Tropsch-type reaction and the hydropyrolysis of oil shale, coal, asphaltene, oil sands, atmospheric residue, vacuum residue, and other heavy fossil-fuel resources.

In our simulation experiments, excess amounts of iron, temperature, and pressure were higher than those in geological settings. In situ studies in existing or depleted wells should be performed in the future for comparison with the simulation results.

Underground in situ combustion, also known as toe-and-heel air injection (THAI), has been applied for residual oil reservoirs after other methods of recoveries, including primary, secondary and enhanced oil recoveries.[4] The combustion is a destructive method, leaving the field essentially char (carbon residue) and becoming unproductive later. The additional of water plus iron into depleted oil wells under high pressure and temperatures could be an alternative to THAI. Our results could also provide some evidence of abiogenic hydrocarbons that could be cogenerated, along with other hydrocarbons believed to be derived from biological origins, based on the evidence of petroleum biomarkers.[53] Abiogenic hydrocarbons have been discovered in space with no evidence of biological presence.

AUTHOR INFORMATION

Corresponding Authors

Hong Lu − *State Key Laboratory of Organic Geochemistry, Guangzhou Institute of Geochemistry, Institutions of Earth Science, Chinese Academic of Sciences, Guangzhou 510640, China*; Email: luhong@gig.ac.cn

Chang Samuel Hsu − *Petro Bio Oil Consulting, Tallahassee, Florida 32312, United States; Department of Chemical and Biomedical Engineering, Florida A&M University/Florida State University, Tallahassee, Florida 32310, United States; State Key Laboratory of Heavy Oil Processing, China University of Petroleum, Beijing, China 102249*; orcid.org/0000-0003-4411-7860; Email: chsu@fsu.edu

Authors

Kang Li − *State Key Laboratory of Organic Geochemistry, Guangzhou Institute of Geochemistry, Institutions of Earth Science, Chinese Academic of Sciences, Guangzhou 510640, China; CAS Center for Excellence in Deep Earth Science, Guangzhou 510640, China; University of Chinese Academy of Sciences, Beijing 100049, China*

Zhongfeng Zhao − *State Key Laboratory of Organic Geochemistry, Guangzhou Institute of Geochemistry, Institutions of Earth Science, Chinese Academic of Sciences, Guangzhou 510640, China; CAS Center for Excellence in Deep Earth Science, Guangzhou 510640, China; University of Chinese Academy of Sciences, Beijing 100049, China*

Ping'an Peng − *State Key Laboratory of Organic Geochemistry, Guangzhou Institute of Geochemistry, Institutions of Earth Science, Chinese Academic of Sciences, Guangzhou 510640, China*

Complete contact information is available at: https://pubs.acs.org/10.1021/acs.energyfuels.1c00284

Notes

The authors declare no competing financial interest.

ACKNOWLEDGMENTS

We express thanks to the two anonymous reviewers for their valuable comments on this article, which makes it better than the earlier version, and we also thank the associate editor Andrew Pomerantz for his patient editing work. We thank Dr. Liangliang Wu for offering the sample of Dalong Formation source rocks. L.H. acknowledges the financial support from the National Key Program of China (No. 2017YFC0603102), the Strategic Priority Research Program of the Chinese Academy of Sciences (No. XDA14010102), National Key Research and Development Project of China (No. 2019YFC0605502), and Chinese NSF grants (Nos. 41973069 and 41673045).

REFERENCES

(1) Vandenbroucke, M.; Largeau, C. Kerogen origin, evolution and structure. *Org. Geochem.* **2007**, *38*, 719−833.
(2) Tissot, B.; Durand, B.; Espitali, J.; Combaz, A. Influence of Nature and Diagenesis of Organic Matter in Formation of Petroleum. *AAPG Bull.* **1974**, *58*, 499−506.
(3) Tissot, B.; Deroo, G.; Hood, A. Geochemical study of the Uinta Basin: formation of petroleum from the Green River formation. *Geochim. Cosmochim. Acta* **1978**, *42*, 1469−1485.
(4) Hsu, C. S.; Robinson, P. R. *Petroleum Science and Technology*; Springer Nature, Switzerland; 2019; p 488.
(5) Galkin, A. A.; Lunin, V. V. Subcritical and Supercritical Water: A Universal Medium for Chemical Reactions. *Russ. Chem. Rev.* **2005**, *74*, 21−35.
(6) Kruse, A.; Dinjus, E. Hot compressed water as reaction medium and reactant:2 Degradation reactions. *J. Supercrit. Fluids* **2007**, *41*, 361−379.
(7) Lewan, M. D. Experiments on the role of water in petroleum formation. *Geochim. Cosmochim. Acta* **1997**, *61*, 3691−3723.
(8) Pan, C.; Geng, A.; Zhong, N.; Liu, J.; Yu, L. Kerogen Pyrolysis in the Presence and Absence of Water and Minerals. 1. Gas Components. *Energy Fuels* **2008**, *22*, 416−427.
(9) Morimoto, M.; Sugimoto, Y.; Saotome, Y.; Sato, S.; Takanohashi, T. J. Effect of supercritical water on upgrading of oil sand bitumen. *J. Supercrit. Fluids* **2010**, *55*, 223−231.
(10) Vilcaez, J.; Watanabe, M.; Watanabe, N.; Kishita, A.; Adschiri, T. Hydrothermal extractive upgrading of bitumen without coke formation. *Fuel* **2012**, *102*, 379−385.
(11) Delbianco, A.; Panariti, N.; Dicarlo, S.; Elmouchnino, J.; Fixari, B.; Leperchec, P. Thermocatalytic hydroconversion of heavy petroleum cuts with dispersed catalyst. *Appl. Catal., A* **1993**, *94*, 1−16.
(12) Rana, M. S.; Samano, V.; Ancheyta, J.; Diaz, J. A. I. A review of recent advances on process technologies for upgrading of heavy oils and residua. *Fuel* **2007**, *86*, 1216−1231.
(13) Arai, K.; Adschiri, T.; Watanabe, M. Hydrogenation of Hydrocarbons through Partial Oxidation in Supercritical Water. *Ind. Eng. Chem. Res.* **2000**, *39*, 4697−4701.
(14) Sato, T.; Mori, S.; Watanabe, M.; Sasaki, M.; Itoh, N. J. Upgrading of bitumen with formic acid in supercritical water. *J. Supercrit. Fluids* **2010**, *55*, 232−240.
(15) Mondragon, F.; Itoh, H.; Ouchi, K. Coal liquefaction by in-situ hydrogen generation. 1. Zinc-water-coal reaction. *Fuel* **1984**, *63*, 968−972.
(16) Fedyaeva, O. N.; Vostrikov, A. A. Hydrogenation of bitumen in situ in supercritical water flow with and without addition of zinc and aluminum. *J. Supercrit. Fluids* **2012**, *72*, 100−110.
(17) Fedyaeva, O. N.; Vostrikov, A. A. Non-isothermal liquefaction of liptobiolith coal in supercritical water flow and effect of zinc additives. *J. Supercrit. Fluids* **2013**, *83*, 86−96.
(18) Fedyaeva, O. N.; Antipenko, V. R.; Shishkin, A. V.; Vostrikov, A. A. Coupled processes of aluminum oxidation and asphaltite hydrogenation in supercritical water flow. *Russ. J. Phys. Chem. B* **2014**, *8*, 1069−1080.
(19) Chen, K.; Li, S.; Zhang, W. Renewable hydrogen generation by bimetallic zero valent iron nanoparticles. *Chem. Eng. J.* **2011**, *170*, 562−567.
(20) Hudson, R.; Hamasaka, G.; Osako, T.; Yamada, Y. M. A.; Li, C.; Uozumi, Y.; Moores, A. Highly efficient iron(0) nanoparticle-catalyzed hydrogenation in water in flow. *Green Chem.* **2013**, *15*, 2141−2148.
(21) Patil, R. D.; Sasson, Y. Generation of Hydrogen from Zero-Valent Iron and Water: Catalytic Transfer Hydrogenation of Olefins in Presence of Pd/C. *Asian J. Org. Chem.* **2015**, *4*, 1258−1261.
(22) Phua, P. H.; Lefort, L.; Boogers, J. A. F.; Tristany, M.; de Vries, J. G. Soluble iron nanoparticles as cheap and environmentally benign alkene and alkyne hydrogenation catalysts. *Chem. Commun.* **2009**, *40*, 3747−3749.
(23) McCollom, T. M.; Lollar, B. S.; Lacrampe-Couloume, G.; Seewald, J. S. The influence of carbon source on abiotic organic synthesis and carbon isotope fractionation under hydrothermal conditions. *Geochim. Cosmochim. Acta* **2010**, *74*, 2717−2740.
(24) De Caprariis, B.; Bavasso, I.; Bracciale, M. P.; Damizia, M.; De Filippis, P.; Scarsella, M. J. Enhanced bio-crude yield and quality by reductive hydrothermal liquefaction of oak wood biomass: effect of iron addition. *J. Anal. Appl. Pyrolysis* **2019**, *139*, 123−130.
(25) Dai, B.; Wu, N.; Wang, J.; Bian, L. Analysis of sedimentary environment of Cambrian Yuertusi source rock in keping uplift, Tarim basin, China. *Fresenius Environ. Bull* **2016**, *38*, 375−381.
(26) Chen, R.-Y.; Zhu, G.-Y.; Zhou, W.-B.; Li, W.; Hu, G.-Y. Geochemical characteristics and hydrocarbon resource potential of Dalong Formation Permian, northeast Sichuan. *Nat. Gas Geosci.* **2013**, *24*, 99−107.
(27) Mao, J.; Fang, X.; Lan, Y.; Schimmelmann, A.; Mastalerz, M.; Xu, L.; Schmidt-Rohr, K. Chemical and nanometer-scale structure of kerogen and its change during thermal maturation investigated by advanced solid-state ^{13}C NMR spectroscopy. *Geochim. Cosmochim. Acta* **2010**, *74*, 2110−2127.
(28) Lu, H.; Greenwood, P.; Chen, T.; Liu, J.; Peng, P. The role of metal sulfates in thermochemical sulfate reduction (TSR) of hydrocarbons: Insight from the yields and stable carbon isotopes of gas products. *Org. Geochem.* **2011**, *42*, 700−706.
(29) Wang, Q.; Lu, H.; Greenwood, P.; Shen, C.; Liu, J.; Peng, P. Gas evolution during kerogen pyrolysis of Estonian Kukersite shale in confined gold tube system. *Org. Geochem.* **2013**, *65*, 74−82.
(30) Pan, C.; Geng, A.; Zhong, N.; Liu, J.; Yu, L. Kerogen pyrolysis in the presence and absence of water and minerals: Amounts and compositions of bitumen and liquid hydrocarbons. *Fuel* **2009**, *88*, 909−919.
(31) Ho, T. A.; Wang, Y.; Xiong, Y.; Criscenti, L. J. Differential retention and release of CO_2 and CH_4 in kerogen nanopores: implications for gas extraction and carbon sequestration. *Fuel* **2018**, *220*, 1−7.
(32) Clarkson, C. R.; Bustin, R. M. Binary gas adsorption/desorption isotherms: effect of moisture and coal composition upon carbon dioxide selectivity over methane. *Int. J. Coal Geol.* **2000**, *42*, 241−271.
(33) Wang, S.; Pomerantz, A. E.; Xu, W.; Lukyanov, A. A.; Kleinberg, R. L.; Wu, Y. S. J. The impact of kerogen properties on shale gas production: a reservoir simulation sensitivity analysis. *J. Nat. Gas Sci. Eng.* **2017**, *48*, 13−23.
(34) Pathak, M.; Huang, H.; Meakin, P.; Deo, M. Molecular investigation of the interactions of carbon dioxide and methane with kerogen: Application in enhanced shale gas recovery. *J. Nat. Gas Sci. Eng.* **2018**, *51*, 1−8.
(35) Krooss, B.M; van Bergen, F; Gensterblum, Y; Siemons, N; Pagnier, H.J.M; David, P High-pressure methane and carbon dioxide adsorption on dry and moisture-equilibrate pennsylvanian coals. *Int. J. Coal Geol.* **2002**, *51*, 69−92.
(36) Wang, W.; Wang, S.; Ma, X.; Gong, J. Recent advances in catalytic hydrogenation of carbon dioxide. *Chem. Soc. Rev.* **2011**, *40*, 3703−3727.
(37) Guo, L.; Sun, J.; Ge, Q.; Tsubaki, N. Recent advances in direct catalytic hydrogenation of carbon dioxide to valuable C_{2+} hydrocarbons. *J. Mater. Chem. A* **2018**, *6*, 23244−23262.
(38) De Smit, E.; Weckhuysen, B. M. The renaissance of iron-based Fischer−Tropsch synthesis: on the multifaceted catalyst deactivation behaviour. *Chem. Soc. Rev.* **2008**, *37*, 2758−2781.
(39) Zhang, Q.; Kang, J.; Wang, Y. Development of Novel Catalysts for Fischer−Tropsch Synthesis: Tuning the Product Selectivity. *ChemCatChem* **2010**, *2*, 1030−1058.
(40) Galvis, H. M. T.; Bitter, J. H.; Khare, C. B.; Ruitenbeek, M.; Dugulan, A. I.; de Jong, K. P. Supported Iron Nanoparticles as Catalysts for Sustainable Production of Lower Olefins. *Science* **2012**, *335*, 835−838.
(41) Al-Dossary, M.; Ismail, A. A.; Fierro, J. L. G.; Bouzid, H.; Al-Sayari, S. A. Effect of Mn loading onto MnFeO nanocomposites for the CO_2 hydrogenation reaction. *Appl. Catal., B* **2015**, *165*, 651−660.
(42) Tannenbaum, E.; Kaplan, I. R. Low-Mr hydrocarbons generated during hydrous and dry pyrolysis of kerogen. *Nature* **1985**, *317*, 708−709.

https://doi.org/10.1021/acs.energyfuels.1c00284
Energy Fuels 2021, 35, 7808−7818

(43) Wang, J.; You, Z.; Zhang, Q.; Deng, W.; Wang, Y. Synthesis of lower olefins by hydrogenation of carbon dioxide over supported iron catalysts. *Catal. Today* **2013**, *215*, 186−193.
(44) Hwang, S. M.; Zhang, C.; Han, S.; Park, H. G.; Kim, Y. T.; Yang, S. K.; Jun, K. W.; Kim, S. K. Mesoporous carbon as an effective support for Fe catalyst for CO_2 hydrogenation to liquid hydrocarbons. *J. CO_2 Util* **2020**, *37*, 65−73.
(45) Hu, Y. N.; Devegowda, D.; Striolo, A.; Van Phan, A. T.; Ho, T. A.; Civan, F.; Sigal, R. Microscopic Dynamics of Water and Hydrocarbon in Shale-Kerogen Pores of Potentially Mixed Wettability. *SPE J.* **2015**, *20*, 112−124.
(46) Ruppert, L. F.; Sakurovs, R.; Blach, T. P.; He, L.; Melnichenko, Y. B.; Mildner, D. F. R.; Alcantar-Lopez, L. A USANS/SANS study of the accessibility of pores in the Barnett shale to methane and water. *Energy Fuels* **2013**, *27*, 772−779.
(47) Behar, F.; Lorant, F.; Budzinski, H.; Desavis, E. Thermal stability of alkylaromatics in natural systems: Kinetics of thermal decomposition of dodecylbenzene. *Energy Fuels* **2002**, *16*, 831−841.
(48) Sanford, E. C. Molecular approach to understanding residuum conversion. *Ind. Eng. Chem. Res.* **1994**, *33*, 109−117.
(49) Sanford, E. C. Conradson carbon residue conversion during hydrocracking of Athabasca Bitumen: catalyst mechanism and deactivation. *Energy Fuels* **1995**, *9*, 549−559.
(50) Weitkamp, J.; Raichle, A.; Traa, Y.; Rupp, M.; Fuder, F. Direct conversion of aromatics into a synthetic steam cracker feed using bifunctional zeolite catalysts. *Chem. Commun.* **2000**, *13*, 1133−1134.
(51) Huang, Z.; Liang, T.; Zhan, Z.; Zou, Y.; Li, M.; Peng, P. Chemical structure evolution of kerogen during oil generation. *Mar. Pet. Geol.* **2018**, *98*, 422−436.
(52) Stanislaus, A.; Cooper, B. H. Aromatic Hydrogenation Catalysis: A Review. *Catal. Rev.: Sci. Eng.* **1994**, *36*, 75−123.
(53) Walters, C. C. Origin of Petroleum. In *Springer Handbook of Petroleum Technology*: Hsu, C. S., Robinson, P. R., Eds.; Springer: New York, 2017; Chapter 10, pp 359−379.

https://doi.org/10.1021/acs.energyfuels.1c00284
Energy Fuels 2021, 35, 7808−7818